JOURNAL OF GUIDANCE, CONTROL, AND DYNAMICS
Vol. 28, No. 2, March–April 2005

Low-Thrust Variable-Specific-Impulse Transfers and Guidance to Unstable Periodic Orbits

Juan Senent* and Cesar Ocampo†
University of Texas at Austin, Austin, Texas 78712
and
Antonio Capella‡
Universitat Politècnica de Catalunya, 08028 Barcelona, Spain

The use of a power-limited, variable-specific-impulse propulsion system to transfer a vehicle from the smaller primary to an arbitrary circular restricted three-body trajectory and the subsequent guidance along all phases of the complete trajectory is investigated. As a practical application, the transfer of a spacecraft with a finite-burn propulsion system from a low Earth orbit to the stable manifold associated with halo and vertical figure-eight orbits at the interior collinear libration point of the sun–Earth/moon system is considered. We find that an indirect method coupled with an adjoint control transformation yields a robust and efficient solution method to construct these transfers. State-feedback linearization for guidance along the powered arcs is able to adjust the control to cancel a range of sinusoidal perturbations. The dynamics of the spacecraft in the sun–Earth/moon system is approximated as a circular restricted three-body problem.

Introduction

OPTIMAL transfers for a spacecraft in a circular restricted three-body problem (CRTBP) force-field model using a variable-specific-impulse (VSI) engine are considered in this study. Applications include both transfers between arbitrary orbits and guidance of the transfer trajectory. Specifically, transfers from a parking orbit around the smaller primary to a periodic orbit at the L1 collinear libration point are examined. As examples, transfers from a near-Earth parking orbit to either a halo orbit or a vertical figure-eight orbit at the L1 libration point of the simplified sun–Earth/moon CRTBP model are presented. The techniques used are general so they can be applied to similar problems in the same context. The main idea is to use the stable invariant manifold of the target orbit as the target constraint manifold from the near-Earth parking orbit. Arriving at the stable manifold and shutting down the engine then guarantees arrival to the unstable periodic orbit some time later if no unmodeled perturbations are present. The nominal trajectory consists of a powered phase between the starting orbit and the stable manifold, followed by an unpowered ballistic phase on the stable manifold. Having established the two phases of the nominal trajectory, the problem of guiding the vehicle along each of these phases is examined. Optimal control theory[1,2] and its application to the optimization of spacecraft trajectories[3,4] is used to solve the optimal finite-burn transfer problem; state feedback linearization (FL)[5] is used to address the guidance phase of the problem, and dynamical systems theory[6] is applied to periodic orbits in the CRTBP model[7] in order to construct and parameterize the stable manifolds of the target periodic orbits.

Presented as Paper 2003-0633 at the AAS/AIAA Astrodynamics Specialist Conference, Big Sky, MT, 4–7 August 2003; received 10 November 2003; revision received 28 May 2004; accepted for publication 1 June 2004. Copyright © 2004 by the American Institute of Aeronautics and Astronautics, Inc. All rights reserved. Copies of this paper may be made for personal or internal use, on condition that the copier pay the $10.00 per-copy fee to the Copyright Clearance Center, Inc., 222 Rosewood Drive, Danvers, MA 01923; include the code 0731-5090/05 $10.00 in correspondence with the CCC.

*Research Scientist, Department of Aerospace Engineering and Engineering Mechanics, 1 University Station C0600; senent@csr.utexas.edu.

†Assistant Professor, Department of Aerospace Engineering and Engineering Mechanics, 1 University Station C0600; cesar.ocampo@mail.utexas.edu.

‡Graduate Student, Departament de Matemàtica Aplicada I; acapella@math.utexas.edu.

Aspects of the problem have been considered previously by numerous investigators, among them Breakwell and Brown,[8] who examined the differential correction procedures for generating families of halo orbits in the Earth–moon system, and Gomez et al.,[7] who considered the use of the stable manifolds of halo orbits in the sun–Earth system as a way to construct transfer trajectories to them. Many articles discuss impulsive transfers to these orbits and their manifolds,[7,9] optimal control theory has been used for impulsive transfers to halo orbits,[10] and finally direct methods have been applied to construct suboptimal low-thrust transfers in the region surrounding the Earth and the collinear libration points[11,12]; to our knowledge, a rigorous analysis using optimal control theory to define the multipoint boundary-value problem for long-duration finite burns and variable specific engines for transfers between the Earth and periodic orbits at the libration points has not been published. Whiffen et al. have used a sophisticated direct method solution to optimal low thrust transfers. Their final solutions seem to take advantage of the unstable properties associated with libration points and their orbits, but they do not use the dynamical systems properties of these orbits directly in their formulation.

In this paper, we show that the use of indirect methods for solving this optimal control problem is robust and efficient provided it is used with a robust nonlinear root finder and provisions are made to facilitate the estimation of the initial value of the unknown variables. Further, we rigorously derive the transversality conditions associated with determining the optimal insertion point on the manifold. Control techniques for guidance and stationkeeping for unstable periodic orbits, such as halo orbits, can found in the literature; these include invariant manifold tracking,[13] Lyapunov exponents and linear quadratic control,[14] output-feedback linearization or linear quadratic control[15] among them. State-feedback linearization is the one chosen for this paper. Although the correction maneuvers are not optimal, the main advantage of this technique is that it allows the use of frequency analysis to obtain the tracking performance without further simulations.

Periodic Orbits and Their Manifolds

The equations of motion of a spacecraft in a CRTBP model are described by

$$\boldsymbol{f} = \dot{\boldsymbol{x}} = \begin{pmatrix} \dot{\boldsymbol{r}} \\ \dot{\boldsymbol{v}} \end{pmatrix} = \begin{bmatrix} \boldsymbol{v} \\ \boldsymbol{g}(\boldsymbol{r}) + \boldsymbol{h}(\boldsymbol{v}) \end{bmatrix} \tag{1}$$

Table 1 Parameters of the CRTBP model for the sun/Earth–moon system

Parameter	Description
GM_1	Gravitational parameter for the sun ($1.3271244001798698 \times 10^{11}$ km^3/s)
GM_2	Gravitational parameter for the Earth/moon (4.03503294×10^5 km^3/s)
a_{12}	Distance between the sun and the Earth/moon barycenter (1.49597870×10^8 km)
ω_n	Mean motion of the sun–Earth/moon rotating system ($1.99098670 \times 10^{-7}$ rad/s)

If the coordinates are centered at the small primary, the vector functions $\boldsymbol{g}(\boldsymbol{r})$ and $\boldsymbol{h}(\boldsymbol{v})$ are

$$\boldsymbol{g}(\boldsymbol{r}) = -\frac{GM_1}{|\boldsymbol{r}-\boldsymbol{r}_1|^3}(\boldsymbol{r}-\boldsymbol{r}_1) - \frac{GM_2}{|\boldsymbol{r}|^3}\boldsymbol{r} - \boldsymbol{\omega}_n \times \boldsymbol{\omega}_n \times [\boldsymbol{r} + a_{12}(1-\mu)\boldsymbol{i}] \tag{2}$$

$$\boldsymbol{h}(\boldsymbol{v}) = -2\boldsymbol{\omega}_n \times \boldsymbol{v} \tag{3}$$

where $\mu \equiv GM_2/(GM_1+GM_2)$, the CRTBP mass-ratio parameter, and $\boldsymbol{i}$ is the unit vector $(1, 0, 0)$.

The parameters of the model used in this paper can be found in Table 1. The x axis points in the direction from the larger primary to the smaller primary, the y axis is parallel to the inertial velocity of the smaller primary, and the z axis completes the right-handed system. In this model, the Earth and moon are considered as the small primary and their barycenter orbits the barycenter of the Sun and the combined Earth/Moon mass in a circular orbit. Periodic orbits in the usual rotating frame of the CRTBP exist at all of the libration points of the system.[16] Actual or approximate initial conditions for these orbits can be determined from one of several methods. Two of these methods include a Poincarè section analysis in the vicinity of these points and the linear system analysis of motion near these points.[8,17] These techniques are well known and are not described here. An approximate initial condition for a periodic orbit is refined to an actual initial condition (within some specified tolerance) by examining the linear variations of the state vector along a reference trajectory based on the approximate initial condition. For the dynamical system

$$\dot{\boldsymbol{x}}(\boldsymbol{t}) = \boldsymbol{f}(\boldsymbol{x}) \tag{4}$$

evaluated from $t_0 = 0$ to some $t = t_f$, the final state differential at t_f is given by

$$\mathrm{d}\boldsymbol{x}_f = \boldsymbol{\Phi}(t_f, t_0)\delta\boldsymbol{x}_0 + \dot{\boldsymbol{x}}_f\,\mathrm{d}t_f \tag{5}$$

where the state transition matrix satisfies

$$\dot{\boldsymbol{\Phi}}(t, t_0) = \boldsymbol{F}(\boldsymbol{x}(t))\boldsymbol{\Phi}(t, t_0), \qquad \boldsymbol{\Phi}(t_0, t_0) = \boldsymbol{I}_{6\times 6} \tag{6}$$

and $\boldsymbol{F}$ is the Jacobian of the vector field used as the state propagation matrix,

$$\boldsymbol{F}(\boldsymbol{x}(t)) = \frac{\partial \boldsymbol{f}(\boldsymbol{x})}{\partial \boldsymbol{x}} \tag{7}$$

At the collinear libration points, the symmetry associated with the unthrusted equations of motion facilitates the derivation of the differential correction expression for a subset of the initial conditions and the time period of the orbit by reducing the problem to determining the periodic orbit conditions based on the state values at half the time period of the orbit. Breakwell and Brown[8] outline a differential correction procedure for the determination of the initial conditions for a family of halo orbits in the sun–Earth system. Following their analysis, which is applicable to periodic orbits that are symmetric with respect to the x–z plane, a differential correction procedure for a nonlinear system of the form $\boldsymbol{e} = \boldsymbol{e}(\boldsymbol{z})$ is used to find the parameter vector $\boldsymbol{z}$ to achieve a desired value for $\boldsymbol{e}$. The correction

$$\delta\boldsymbol{z} = \boldsymbol{A}^{-1}\delta\boldsymbol{e}$$

is used iteratively until the norm of $\boldsymbol{e}$ is satisfied to within a specified tolerance. $\boldsymbol{A}$ is the Jacobian matrix of the system. For a periodic orbit that is symmetric with respect to the x–z plane $(\dot{x}_0 \;\; \dot{z}_0) = 0^\top$, $x_0 = x_{\text{specified}}$, $\dot{y}_0$, z_0, t_f, are estimates to be adjusted, and $(y_f, \dot{x}_f, \dot{z}_f) = 0^\top$. The perturbation vectors and the Jacobian matrix for this problem are

$$\delta\boldsymbol{z} = \begin{pmatrix} \delta z_0 \\ \delta \dot{y}_0 \\ \mathrm{d}t_f \end{pmatrix}, \qquad \delta\boldsymbol{e} = \begin{pmatrix} \delta y_f \\ \delta \dot{x}_f \\ \delta \dot{z}_f \end{pmatrix}, \qquad \boldsymbol{A} = \begin{pmatrix} \phi_{23} & \phi_{25} & \dot{y}_f \\ \phi_{43} & \phi_{45} & \ddot{x}_f \\ \phi_{63} & \phi_{65} & \ddot{z}_f \end{pmatrix}$$

where ϕ_{ij} is the i, j, element of $\boldsymbol{\Phi}$. The period of the orbit is $T = 2t_f$, and the state transition matrix evaluated from $t_0 = 0$ to T is the full-cycle state transition matrix known also as the one-revolution monodromy matrix of the periodic orbit; it is denoted by $\boldsymbol{\Phi}(T, 0)$.

Determination and Parameterization of the Stable Manifold

An eigensystem analysis of the monodromy matrix for a periodic orbit in the CRTBP provides a complete description of the behavior of solutions near the periodic orbit.[6] Gomez et al.[7] described completely the eigensystem analysis associated with halo-type orbits, which also applies to other types of unstable CRTBP periodic orbits. For the current study, the hyperbolic behavior of the orbit is of interest and is associated with the two real eigenvalues of the monodromy matrix that do not lie on the unit circle. These eigenvalues λ_u, λ_s have the property that $\lambda_u\lambda_s = 1$, $\lambda_u > 1$, and $\lambda_s < 1$. Their associated eigenvectors are $\boldsymbol{e}_u$ and $\boldsymbol{e}_s$; $\boldsymbol{e}_u$ represents the expanding direction, and $\boldsymbol{e}_s$ represents the contracting direction. Let $\boldsymbol{e}_u(0)$ and $\boldsymbol{e}_s(0)$ represent the eigenvectors evaluated at the starting point of the orbit where $\boldsymbol{x}(0) = \boldsymbol{x}(T)$. The state along the orbit is referenced by a time-like variable τ, which is normalized with respect to the periodic orbit's time period T. The image of the eigenvectors along the orbit is obtained by the linear mapping:

$$\boldsymbol{e}_{u,s}(\tau) = \boldsymbol{\Phi}(\tau, 0)\boldsymbol{e}_{u,s}(0) \tag{8}$$

where $\boldsymbol{\Phi}(0, 0) = \boldsymbol{I}_{6\times 6}$ and $0 \le \tau \le 1$. Because $\boldsymbol{e}_{u,s}(\tau)$ both represent a direction, it is normalized to be a unit vector at every τ. Together with the eigenvector tangent to the orbit (corresponding to the unitary eigenvalues), $\boldsymbol{e}_u(\tau)$ and $\boldsymbol{e}_s(\tau)$ give the tangent plane to the local unstable manifold W^u and the local stable manifold W^s at each point on the orbit. Because of the symmetry of the CRTBP, if $\boldsymbol{e}_u = [v_{u_1}, v_{u_2}, v_{u_3}, v_{u_4}, v_{u_5}, v_{u_6}]^T$ is the eigenvector associated with λ_u then $\boldsymbol{e}_s = [v_{u_1}, -v_{u_2}, v_{u_3}, -v_{u_4}, v_{u_5}, -v_{u_6}]^T$ is the one associated with λ_s, for example,

$$\boldsymbol{e}_s = \boldsymbol{T}\boldsymbol{e}_u \tag{9}$$

where $\boldsymbol{T}$ is a diagonal matrix with elements

$$T_{ii} = \begin{cases} +1 & i \quad \text{odd} \\ -1 & i \quad \text{even} \end{cases} \tag{10}$$

Numerical integration of the equations of motion is used to globalize the manifolds by extending them to other regions in phase space. The stable manifold has two distinct parts: a stable manifold surface from the direction of the larger primary and one from the smaller primary (if the orbit is the interior libration point). The stable manifold from the smaller primary is of interest in the current application. A curve on this manifold is determined by integrating backwards in time by α from an initial perturbed state vector given by

$$\boldsymbol{x}'_M(\tau, 0) = \boldsymbol{x}(\tau) + \varepsilon[\boldsymbol{e}_s(\tau)/e_s(\tau)] = \boldsymbol{x}(\tau) + \varepsilon\boldsymbol{v}_s(\tau) \tag{11}$$

where ε is a small positive number, small enough so that linear approximation to the manifold remains valid (see Refs. 7 and 18 for a detailed discussion on the method and the selection of ε). Phase space points on the curve are given by $\boldsymbol{x}_M(\tau, \alpha)$ and α represents the time to orbit. In summary, the manifold is parameterized by the two time variables, τ and α, where $\tau \in [0, 1]$ and $\alpha \ge 0$. This parameterization is equivalent to that given by Gomez et al.,[7] where τ represents the parameter along the orbit and α is the parameter along the flow. Alternatively, the stable manifold can be generated

by computing a perturbed state based on the normalized eigenvector associated with the unstable direction $[\boldsymbol{v}_u(\tau)]$.

$$\boldsymbol{x}'_M(-\tau, 0) = \boldsymbol{T}\{\boldsymbol{x}(\tau)+\varepsilon[\boldsymbol{e}_u(\tau)/e_u(\tau)]\} = \boldsymbol{T}[\boldsymbol{x}(\tau)+\varepsilon\boldsymbol{v}_u(\tau)] \quad (12)$$

and integrating backwards in time through α as before. The manifold is extended by assuming suitable ranges for $\alpha \in [0, \alpha_{\max}]$.

Target Stable Manifolds for Halo and Vertical Figure-Eight Orbits

Halo orbits in the CRTBP are three-dimensional periodic solutions that exist at all of the collinear libration points of the CRTBP model. At a specific in-plane amplitude, they bifurcate from the planar Lyapunov orbits around the collinear libration points. An individual halo orbit has symmetry with respect to the x–z plane only, and the family of halo orbits has symmetry with respect to the plane of the primaries (the x–y plane). They have been extensively studied in the context of both the sun–Earth and Earth–moon systems.[7,8]

The vertical figure-eight orbits at the collinear libration points are large z-axis amplitude orbits with symmetry with respect to both the x–y and x–z planes.[16] Both the halo and figure-eight orbits serve as the final target orbits in the current study. Figures 1–3 illustrate the

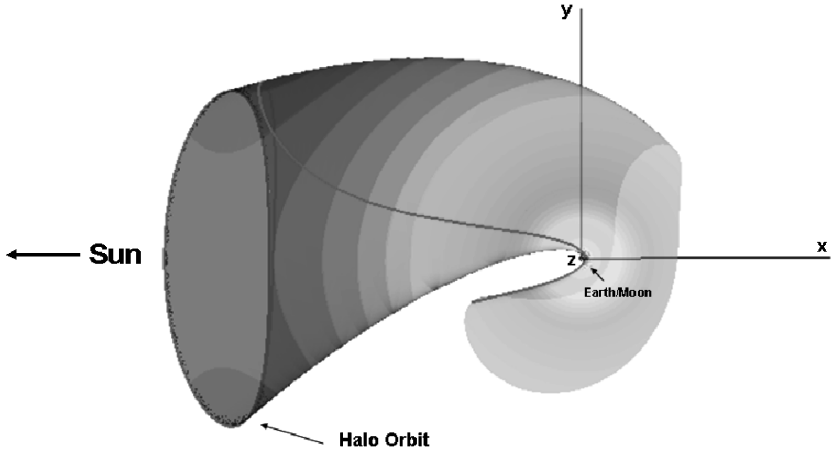

Fig. 1 Halo orbit and part of the stable manifold in configuration space.

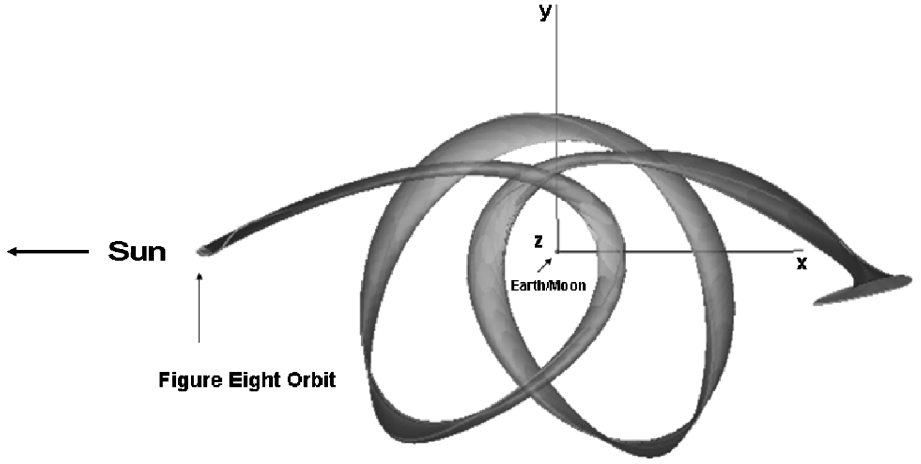

Fig. 2 Top view of the vertical figure-eight orbit and part of its stable manifold in configuration space.

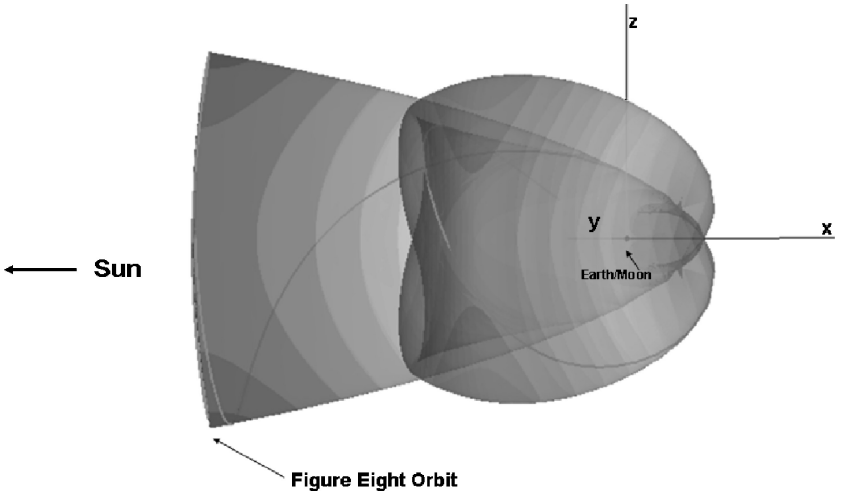

Fig. 3 Side view of the vertical figure-eight orbit and part of its stable manifold in configuration space. This view shows only one periapsis passage.

Table 2 Halo orbit and stable-manifold parameters

Parameter	Value	Unit
x_0	−1,200,000.000	km
z_0	−282,193.8259	km
$\dot{y}_0$	−0.326819256	km/s
T	177.635799	day
τ	$0.00 \rightarrow 1$	units of T
α	$0.00 \rightarrow 350.15$	day

Table 3 Vertical figure-eight and stable-manifold parameters

Parameter	Value	Unit
x_0	−1,404,161.490033	km
z_0	−621,647.510431	km
$\dot{y}_0$	−0.0014216302	km/s
T	183.921464	days
τ	$0.00 \rightarrow 1$	units of T
α	$0.00 \rightarrow 339.94$	days

specific orbits with their associated local stable invariant manifolds from the Earth. Tables 2 and 3 tabulate the data associated with the halo and vertical figure-eight orbits, respectively.

To solve the optimal control problem described in the next section, the stable invariant manifold will not be stored; all that needs to be stored is the initial condition of the periodic orbit and the monodromy matrix. For a given value of the parameters that define a state on the manifold $\boldsymbol{x}_M(\tau, \alpha)$, that point is computed by integrating in real time a curve on the manifold. Because of the nature of the optimization algorithm (it is a local optimizer), it will explore only a region of the manifold; therefore, it is not necessary to store the complete manifold to solve the problem. Storing the manifold might be faster to retrieve the necessary states, but at the expense of memory and required interpolations.

Finite-Burn Optimization of the Parking Orbit to Manifold Phase

Adding the thrust acceleration term, the manifold and parking-orbit parameters to the equations of motion requires augmenting the state vector by including the mass of the spacecraft and the parameters as additional state variables; hence, $\boldsymbol{x} = (\boldsymbol{r}\ \ \boldsymbol{v}\ \ m\ \ \alpha\ \ \tau\ \ \tau_1)^\top$, and the equations of motion become

$$\begin{pmatrix} \dot{\boldsymbol{r}} \\ \dot{\boldsymbol{v}} \\ \dot{m} \\ \dot{\alpha} \\ \dot{\tau} \\ \dot{\tau}_1 \end{pmatrix} = \begin{pmatrix} \boldsymbol{v} \\ \boldsymbol{g}(\boldsymbol{r}) + \boldsymbol{h}(\boldsymbol{v}) + T/m\boldsymbol{u} \\ -T^2/(2P) \\ 0 \\ 0 \\ 0 \end{pmatrix} \tag{13}$$

Here, $\boldsymbol{u}$ is the thrust direction unit vector, T the thrust magnitude, P the power at which the engine operates, α and τ are defined as earlier, and τ_1 is a scalar parametrization of position and velocity of the parking orbit. These last three parameters are added as states, and their time derivatives are necessarily zero.

There are many possible ways in which to form the optimization problem. Because of the nature of low-thrust trajectories, an optimal variable specific low-thrust trajectory that maximizes the final mass m_f can theoretically extend the final time t_f close to infinity. To cut this final time to obtain a feasible solution, the mass ratio m_f/m_0 will be fixed. Therefore, it has been assumed that the vehicle has a fixed and known propellant mass and that it is desired to move it from its parking orbit at the small primary to the stable manifold in minimum time. The time along the manifold is not included in the cost. The cost is given by $J = \max -kt_f$ $(k > 0)$, and the optimal control Hamiltonian and the costate equations for the system are given by

$$H = \boldsymbol{\lambda}_r^\top \boldsymbol{v} + \boldsymbol{\lambda}_v^\top \left[\boldsymbol{g}(\boldsymbol{r}) + \boldsymbol{h}(\boldsymbol{v}) + \frac{T}{m}\boldsymbol{u} \right] + \lambda_m \left(-\frac{T^2}{2P_{\max}} \right) + \lambda_\alpha \cdot 0 + \lambda_\tau \cdot 0 + \lambda_{\tau_1} \cdot 0 \tag{14}$$

$$\dot{\boldsymbol{\lambda}} = -\left(\frac{\partial H}{\partial \boldsymbol{x}} \right)^\top = \begin{pmatrix} \dot{\boldsymbol{\lambda}}_r \\ \dot{\boldsymbol{\lambda}}_v \\ \dot{\lambda}_m \\ \dot{\lambda}_\alpha \\ \dot{\lambda}_\tau \\ \dot{\lambda}_{\tau_1} \end{pmatrix} = \begin{pmatrix} -\left(\frac{\partial \boldsymbol{g}}{\partial \boldsymbol{r}} \right)^\top \boldsymbol{\lambda}_v \\ -\boldsymbol{\lambda}_r - \left(\frac{\partial \boldsymbol{h}}{\partial \boldsymbol{v}} \right)^\top \boldsymbol{\lambda}_v \\ \frac{T}{m^2} \boldsymbol{\lambda}_v^\top \boldsymbol{u} \\ 0 \\ 0 \\ 0 \end{pmatrix} \tag{15}$$

The controls are $\boldsymbol{u}$, T, and P. The unit thrust direction $\boldsymbol{u}$ is constrained to the unit sphere, the thrust magnitude is unconstrained, But the power to the engine is constrained by

$$0 \le P \le P_{\max} \tag{16}$$

This is a simple model that excludes thrust and I_{sp} constraints. However, it is the basis for more complex propulsion system models that have been considered previously for variable specific impulse systems in a generalized trajectory optimization system.[19]

Maximization of the Hamiltonian[20] with respect to the controls $T, \boldsymbol{u}, P$ yields the well-known first-order control optimality conditions:

$$P = P_{\max}, \qquad T = \frac{\lambda_v P_{\max}}{\lambda_m m}, \qquad \boldsymbol{u} = \frac{\boldsymbol{\lambda}_v}{\lambda_v} \tag{17}$$

The departing point on the initial orbit is given by the six-dimensional state vector $\boldsymbol{x}_D(\tau_1)$. It is parameterized by the time-like variable τ_1 referenced from the epoch of the orbit's initial state $\boldsymbol{x}_{D_0}$ that defines the parking orbit. The state at τ_1 is determined from a numerical propagation of the uncontrolled equations of motion from the orbit initial epoch to τ_1.

The arrival point on the manifold is the target state for the spacecraft and is given by $\boldsymbol{x}_M(\tau, \alpha)$. The orbit transfer is a time-free transfer of a spacecraft between a circular near-Earth orbit and the stable manifold of the target unstable orbit. The epoch at the arrival point on the manifold is given by t_f. All of the time variables $\tau_1, t_f, \tau, \alpha$ are independent optimization variables and the initial time is set to $t_0 = 0$ when $\boldsymbol{x}(t_0) = \boldsymbol{x}(\tau_1)$.

With these definitions the kinematic boundary conditions are given by

$$\boldsymbol{\theta}(t_0, \boldsymbol{x}_0) = \begin{pmatrix} \boldsymbol{r}(t_0) - \boldsymbol{r}_D(\tau_{1_0}) \\ \boldsymbol{v}(t_0) - \boldsymbol{v}_D(\tau_{1_0}) \\ m(t_0) - m_0 \end{pmatrix} = 0 \tag{18}$$

$$\boldsymbol{\psi}(t_f, \boldsymbol{x}(t_f)) = \begin{pmatrix} \boldsymbol{r}(t_f) - \boldsymbol{r}_M(\tau_f, \alpha_f) \\ \boldsymbol{v}(t_f) - \boldsymbol{v}_M(\tau_f, \alpha_f) \\ m(t_f) - m_f \end{pmatrix} = 0 \tag{19}$$

These initial and final state constraints are adjoined to the Bolza function via an additional set of Lagrange multipliers

$$G = G(t_0, t_f, \boldsymbol{x}(t_0), \boldsymbol{x}(t_f), \boldsymbol{\omega}, \boldsymbol{\nu}) = -kt_f + \boldsymbol{\omega}^\top \boldsymbol{\theta}(t_0, \boldsymbol{x}(t_0)) + \boldsymbol{\nu}^\top \boldsymbol{\psi}(t_f, \boldsymbol{x}(t_f)) \tag{20}$$

Equation (18) can be inherently satisfied by setting τ_1 and choosing $\boldsymbol{x}_0$ as the result of propagating $\boldsymbol{x}_{D_0}$ for τ_1 units. The remaining transversality conditions are determined by nulling the differential

of the cost with respect to the independent time variables; the general form of the differential of the cost is given as[3]

$$\mathrm{d}J' = \mathrm{d}G + (H\,\mathrm{d}t - \boldsymbol{\lambda}^\top \mathrm{d}\boldsymbol{x})_{t_0}^{t_f} = 0 \tag{21}$$

This expression is expanded in terms of the chosen optimization variables

$$\mathrm{d}G = \frac{\partial G}{\partial t_0}\,\mathrm{d}t_0 + \frac{\partial G}{\partial t_f}\,\mathrm{d}t_f + \frac{\partial G}{\partial x(t_0)}\,\mathrm{d}\boldsymbol{x}(t_0) + \frac{\partial G}{\partial \boldsymbol{x}(t_f)}\,\mathrm{d}\boldsymbol{x}(t_f) + \frac{\partial G}{\partial \boldsymbol{\omega}}\,\mathrm{d}\boldsymbol{\omega} + \frac{\partial G}{\partial \boldsymbol{\nu}}\,\mathrm{d}\boldsymbol{\nu}$$

Setting the coefficients of each of the independent time variable differentials results in the transversality conditions; the trivial ones are

$$\boldsymbol{\lambda}_{r_0,v_0,m_0} = -\boldsymbol{\omega}, \qquad \boldsymbol{\lambda}_{r_f,v_f,m_f} = \boldsymbol{\nu} \tag{22}$$

which are then used to form the final set of conditions used to construct the constraint vector

$$H_f = k \tag{23}$$

$$\boldsymbol{\lambda}_{r_0,v_0}^\top \frac{\partial \boldsymbol{x}_D(\tau_{1_0})}{\partial \tau_{1_0}} = 0 \tag{24}$$

$$\begin{bmatrix} \boldsymbol{r}(t_0) - \boldsymbol{r}_D(\tau_{1_0}) \\ \boldsymbol{v}(t_0) - \boldsymbol{v}_D(\tau_{1_0}) \\ m(t_0) - m_0 \end{bmatrix} = \boldsymbol{0} \tag{25}$$

$$\boldsymbol{\lambda}_{r_f,v_f}^\top \frac{\partial \boldsymbol{x}_M(\tau_f,\alpha_f)}{\partial \alpha_f} = 0 \tag{26}$$

$$\boldsymbol{\lambda}_{r_f,v_f}^\top \frac{\partial \boldsymbol{x}_M(\tau_f,\alpha_f)}{\partial \tau_f} = 0 \tag{27}$$

$$\begin{bmatrix} \boldsymbol{r}(t_f) - \boldsymbol{r}_M(\tau_f,\alpha_f) \\ \boldsymbol{v}(t_f) - \boldsymbol{v}_M(\tau_f,\alpha_f) \\ m(t_f) - m_f \end{bmatrix} = \boldsymbol{0} \tag{28}$$

yielding a set of 18 constraint functions; a further procedure to be discussed in the next section reduces the dimension by eight.

Figures 4 and 5 show the differentials of both α and τ for a trajectory on the manifold of the periodic orbit. Note that $\dot{\alpha}, \dot{\tau}, \dot{\tau}_1$ are zero, so that $\alpha_0 = \alpha_f = \alpha$, $\tau_0 = \tau_f = \tau$, and $\tau_{1_0} = \tau_{1_f} = \tau_1$:

$$\frac{\partial \boldsymbol{x}_M(\tau,\alpha)}{\partial \alpha} = \boldsymbol{f}(\boldsymbol{x}_M(\tau,\alpha))\frac{\mathrm{d}t}{\mathrm{d}\alpha} \tag{29}$$

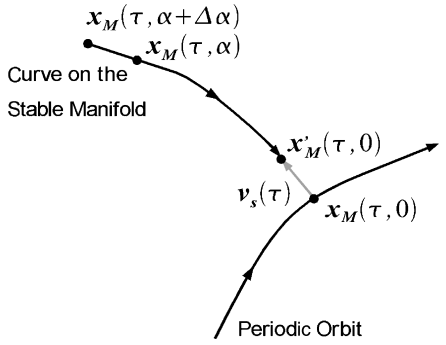

Fig. 4 Geometry associated with the gradient of the state on the manifold with respect to α.

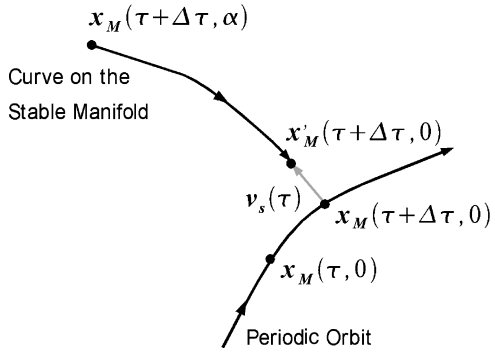

Fig. 5 Geometry associated with the gradient of the state on the manifold with respect to τ.

To obtain an expression for $\partial \boldsymbol{x}_M(\tau,\alpha)/\partial\tau$, some auxiliary variables are used (see Fig. 5). If $\boldsymbol{x}'_M(\tau, 0)$ is calculated using Eq. (11),

$$\frac{\partial \boldsymbol{x}'_M(\tau,0)}{\partial \tau} = \boldsymbol{f}(\boldsymbol{x}_M(\tau,0))\frac{\mathrm{d}t}{\mathrm{d}\tau} + \epsilon\frac{\partial \boldsymbol{v}_s(\tau)}{\partial \tau} \tag{30}$$

$$\frac{\partial \boldsymbol{v}_s(\tau)}{\partial \tau} = \left[\boldsymbol{I} - \boldsymbol{v}_s(\tau)\boldsymbol{v}_s(\tau)^\top\right]\boldsymbol{F}(\boldsymbol{x}_M(\tau,0))\boldsymbol{v}_s(\tau)\frac{\mathrm{d}t}{\mathrm{d}\tau} \tag{31}$$

where $\boldsymbol{\Phi}(\tau, 0)$ is the state transition matrix evaluated from 0 to τ and the initial state on the periodic orbit is $\boldsymbol{x}_M(0, 0)$.

$$\frac{\partial \boldsymbol{x}_M(\tau,\alpha)}{\partial \boldsymbol{x}'_M(\tau,0)} = \boldsymbol{\Phi}(\alpha, 0) \tag{32}$$

where $\boldsymbol{\Phi}(\alpha, 0)$ is the state transition matrix evaluated from 0 to $-\alpha$ and the initial state is $\boldsymbol{x}'_M(\tau, 0)$.

$$\frac{\partial \boldsymbol{x}_M(\tau,\alpha)}{\partial \tau} = \boldsymbol{\Phi}(\alpha,0)\Big[\boldsymbol{f}(\boldsymbol{x}_M(\tau,0)) + \epsilon\left[\boldsymbol{I} - \boldsymbol{v}_s(\tau)\boldsymbol{v}_s(\tau)^\top\right]\boldsymbol{F}(\boldsymbol{x}_M(\tau,0))\boldsymbol{v}_s(\tau)\Big]\frac{\mathrm{d}t}{\mathrm{d}\tau} \tag{33}$$

The finite-burn transfer from the parking orbit to the stable manifold of the target orbit is then reduced to a two-point boundary-value problem with floating terminal points whose parameters form part of the search vector. The problem is solved with a nonlinear root-finding algorithm or a nonlinear programming algorithm.

Adjoint-Control Transformation

To reduce sensitivity to the initial estimates of the Lagrange multipliers $\boldsymbol{\lambda}_0$, an adjoint control transformation (ACT)[21] is used. The objective is to obtain an initial estimate of $\boldsymbol{\lambda}_0$ using a set of control-related variables that are less sensitive to the initial state $\boldsymbol{x}_0$. For convenience, a vehicle-centered coordinate system is defined where the velocity direction is the x axis, the z axis is along the instantaneous angular momentum vector with respect to the Earth, and the y axis completes the right-handed system. This system is referred to as the vuw frame, and its unit vector definitions are given by

$$\hat{\boldsymbol{v}} \equiv \frac{\boldsymbol{v}}{v}, \qquad \hat{\boldsymbol{w}} \equiv \frac{\boldsymbol{r}\times\boldsymbol{v}}{|\boldsymbol{r}\times\boldsymbol{v}|}, \qquad \hat{\boldsymbol{u}} \equiv \hat{\boldsymbol{w}}\times\hat{\boldsymbol{v}} \tag{34}$$

In this frame, the thrusting pointing unit vector $\boldsymbol{u}'$ and its derivative $\dot{\boldsymbol{u}}'$ can be parameterized by two orientation angles (ρ, δ) and their rates $(\dot{\rho}, \dot{\delta})$, where ρ is in plane $(\hat{\boldsymbol{v}} - \hat{\boldsymbol{u}})$ measured positive away from $\hat{\boldsymbol{v}}$, and δ is out of plane (elevation) above or below the $\hat{\boldsymbol{v}} - \hat{\boldsymbol{u}}$ plane:

$$\boldsymbol{u}' = \begin{bmatrix} \cos\rho\cos\delta \\ \sin\rho\cos\delta \\ \sin\delta \end{bmatrix}, \qquad \dot{\boldsymbol{u}}' = \begin{bmatrix} -\dot{\rho}\sin\rho\cos\delta - \dot{\delta}\cos\rho\sin\delta \\ \dot{\rho}\cos\rho\cos\delta - \dot{\delta}\sin\rho\sin\delta \\ \dot{\delta}\cos\delta \end{bmatrix} \tag{35}$$

These are then represented in the CRTBP ijk frame via the transformations

$$\boldsymbol{u}_0 = \boldsymbol{R}_0 \boldsymbol{u}_0' \tag{36}$$

$$\dot{\boldsymbol{u}}_0 = \boldsymbol{R}_0 \dot{\boldsymbol{u}}_0' + \dot{\boldsymbol{R}}_0 \boldsymbol{u}_0' \tag{37}$$

where $\boldsymbol{R}$ is the direction cosine transformation matrix from the vuw frame to the original frame and $\dot{\boldsymbol{R}}$ is its first time derivative.

The transformation to the desired costate vectors $(\boldsymbol{\lambda}_r, \boldsymbol{\lambda}_v)$ at t_0 uses the control optimality condition, the constraint on the Hamiltonian, and the transversality condition on the initial departure point on the parking orbit [(Eq. 23)] and is summarized as

$$\boldsymbol{\lambda}_v = \lambda_v \boldsymbol{u} \tag{38}$$

$$\boldsymbol{\lambda}_r = -\dot{\boldsymbol{\lambda}}_v - \frac{\partial \boldsymbol{h}}{\partial \boldsymbol{v}}^{\top} \boldsymbol{\lambda}_v \tag{39}$$

where

$$\dot{\boldsymbol{\lambda}}_v = \dot{\lambda}_v \boldsymbol{u} + \lambda_v \dot{\boldsymbol{u}} \tag{40}$$

$$\dot{\lambda}_v = -\frac{1}{\boldsymbol{u}^{\top}\boldsymbol{v}} \left[\lambda_v \dot{\boldsymbol{u}}^{\top} \boldsymbol{v} + \boldsymbol{\lambda}_v^{\top} \frac{\partial \boldsymbol{h}}{\partial \boldsymbol{v}} \boldsymbol{v} - \boldsymbol{\lambda}_v^{\top} (\boldsymbol{g} + \boldsymbol{h}) \right] \tag{41}$$

With this transformation the search variables are $(\lambda_v, \lambda_m, \rho, \delta, \dot{\rho}, \dot{\delta}, \tau_1, \tau, \alpha, t_f)$; it is a vector composed of elements with a more physical significance and, as such, is easier to estimate. The sensitivity of solution to an initial estimate is also reduced because $\boldsymbol{\lambda}_r$ and $\boldsymbol{\lambda}_v$ are now insensitive to large changes in τ_1 because of the representation of the thrust vector in the vuw frame. The finite-burn transfer phase is then reduced to well-defined boundary-value problem of dimension 10. The constraint vector is now given by

$$\begin{pmatrix} e_x \\ e_y \\ e_z \\ e_{\dot{x}} \\ e_{\dot{y}} \\ e_{\dot{z}} \\ e_{\mathrm{mf}} \\ e_{H_f} \\ e_{M1} \\ e_{M2} \end{pmatrix} = \begin{bmatrix} r_x(t_f) - r_{Mx}(\tau_f, \alpha_f) \\ r_y(t_f) - r_{My}(\tau_f, \alpha_f) \\ r_z(t_f) - r_{Mz}(\tau_f, \alpha_f) \\ v_x(t_f) - v_{Mx}(\tau_f, \alpha_f) \\ v_y(t_f) - v_{My}(\tau_f, \alpha_f) \\ v_z(t_f) - v_{Mz}(\tau_f, \alpha_f) \\ m(t_f) - m_f \\ H_f - k \\ \boldsymbol{\lambda}_{r_f, v_f}^{\top} \dfrac{\partial \boldsymbol{x}_M(\tau_f, \alpha_f)}{\partial \alpha_f} \\ \boldsymbol{\lambda}_{r_f, v_f}^{\top} \dfrac{\partial \boldsymbol{x}_M(\tau_f, \alpha_f)}{\partial \tau_f} \end{bmatrix}$$

An additional relationship that can be used as part of the ACT or as an independent check is the following: by using Eq. (23) and the fact that $H_f = 1$ (when $k = 1$) and $\dot{H} = 0$,

$$\boldsymbol{\lambda}_{v_0} = \sqrt{2(m_0)^2 \lambda_{m_0} \big/ P_{\max}} \tag{42}$$

Guidance Along Powered Arcs

The finite-burn solution is open loop and requires guidance. The guidance of this powered arc is carried out by a nonlinear control law based on FL.[5] The objective is to design a real-time controller to track the nominal and optimal trajectory under the presence of perturbations. The controller adjusts the thrust vector in the presence of perturbations on the nominal trajectory.

If the state error at time t is defined as

$$\boldsymbol{e}(t) = \begin{bmatrix} \boldsymbol{e}_r(t) \\ \boldsymbol{e}_v(t) \end{bmatrix} = \begin{bmatrix} \boldsymbol{r}(t) - \boldsymbol{r}^*(t) \\ \boldsymbol{v}(t) - \boldsymbol{v}^*(t) \end{bmatrix} \tag{43}$$

where $\boldsymbol{r}^*(t)$ and $\boldsymbol{v}^*(t)$ are the optimal position and velocity of the nominal trajectory and $\boldsymbol{r}(t)$ and $\boldsymbol{v}(t)$ are the current state vector of spacecraft provided by the orbit estimation and navigation system. The variations of the error with respect to time are

$$\begin{pmatrix} \dot{\boldsymbol{e}}_r \\ \dot{\boldsymbol{e}}_v \end{pmatrix} = \begin{bmatrix} \boldsymbol{v} - \boldsymbol{v}^* \\ \boldsymbol{g}(\boldsymbol{r}) + \boldsymbol{h}(\boldsymbol{v}) + \dfrac{\boldsymbol{T}}{m} - \dot{\boldsymbol{v}}^* \end{bmatrix} \tag{44}$$

where $\boldsymbol{T} = T\boldsymbol{u}$. The control law is defined as

$$\boldsymbol{T} = m[\dot{\boldsymbol{v}}^* - \boldsymbol{g}(\boldsymbol{r}) - \boldsymbol{h}(\boldsymbol{v}) + \boldsymbol{u}_L] \tag{45}$$

where $\boldsymbol{u}_L$ is an auxiliary control input. Using this control law in Eq. (44), the system is linearized:

$$\begin{pmatrix} \dot{\boldsymbol{e}}_r \\ \dot{\boldsymbol{e}}_v \end{pmatrix} = \begin{pmatrix} 0 & \boldsymbol{I} \\ 0 & 0 \end{pmatrix} \begin{pmatrix} \boldsymbol{e}_r \\ \boldsymbol{e}_v \end{pmatrix} + \begin{pmatrix} 0 \\ \boldsymbol{I} \end{pmatrix} \boldsymbol{u}_L \tag{46}$$

A linear control law can be designed with the form

$$\boldsymbol{u}_L = \boldsymbol{K} \begin{pmatrix} \boldsymbol{e}_r \\ \boldsymbol{e}_v \end{pmatrix} \tag{47}$$

such that the closed loop is stable and satisfies time specifications (i.e., time to return to the optimal trajectory) or frequency specifications (i.e., rejection of disturbances in a determined bandwidth). $\boldsymbol{K}$ can be designed using well-known techniques from the linear control theory (pole placement, optimal control, etc.). [If $\boldsymbol{K}$ is designed using optimal control theory, the linear controller will be optimal, but the nonlinear control law in Eq. (45) is not necessarily optimal.]

Finally, all of the information that is necessary to carry out the guidance is the current position and velocity of the spacecraft and the acceleration $\dot{\boldsymbol{v}}^*(t)$ along the optimal trajectory. In the case of powered arcs

$$\dot{\boldsymbol{v}}^*(t) = \boldsymbol{g}(\boldsymbol{r}^*) + \boldsymbol{h}(\boldsymbol{v}^*) + [T(t)^*/m(t)^*]\boldsymbol{u}(t)^* \tag{48}$$

where starred superscripts denote the reference values.

Transfer and Guidance Examples

The results for two variable-specific-impulse transfer examples and two guidance examples are described in this section. The transfer examples include VSI transfers from a chosen near-Earth orbit to the stable manifolds of the halo and vertical figure-eight orbits already described. The two guidance examples are associated with the halo orbit transfer mission only. The guidance examples will consider unmodeled perturbing accelerations along the three-axis components with distinct frequencies and amplitudes. These perturbing accelerations are unknown to the controller. The purpose of these examples is to illustrate the methodology described and is not intended to be a comprehensive numerical study; they are provided as a proof of concept and as a basis for future investigations.

The transfer optimization problems are solved by using either one of two methods. In the first, the nonlinear multipoint boundary-value problem is solved as a system of nonlinear equations. The method uses the ideas of Newton–Raphson and steepest descent, coupled with Broyden's method for improving Jacobian matrices. In the second, a sequential-quadratic-programming algorithm is used. In this case the transversality conditions on the costates are not used, and only the kinematic boundary constraints are treated as equality constraints, while the cost is set to minimize the transfer time to the manifold. In both methods, the control is based on the first-order control optimality condition. Both methods have been implemented using the Harwell Subroutine Library.[22] The integration method implemented for the simulation is a Runge–Kutta7/8 with relative error tolerance equal to 10^{-11}. (Absolute error tolerance was not used.) Finally, for the generation of the stable invariant manifold $\varepsilon = 10^{-8}$ (in normalized coordinates) has been chosen. In this way the position error in the insertion point IP_{error} of the periodic orbit is $IP_{\mathrm{error}} \leq \varepsilon \cdot a_{12} = 1.4959$ km.

As for the starting (parking) orbit for the transfer examples, the Earth and the moon are represented as one body; the starting parking orbit about this body is adjusted to approximate the effect of the moon in the calculation of the departure trajectory. The approximation used follows Pu and Edelbaum,[23] whereby the initial radius corresponds to a circular orbit velocity that is equal to the circular orbit velocity about the Earth only at the nominal semimajor axis; the proper transformation to the rotating coordinate system then yields the magnitude velocity required in rotating coordinates. The parking orbit in this study is assumed to be confined to the x–y plane with a starting coordinate on the x axis given by x_0 that corresponds to the adjusted semimajor axis value (20246.0486681 km); the orbit is not necessarily periodic in the rotating coordinate system and the departure point is given by τ_1, a free parameter.

The first set of transfer examples is associated with a transfer to a halo orbit at the interior libration point L_1 of the sun–Earth/moon system. Two different transfer examples are shown in Figs. 6 and 7. These are followed by figures showing the control variables T, ρ, δ along the powered arc and the mass variation (Figs. 8 and 9). Tables 4 and 5 show the parameters specific with these transfers. These transfer examples represent two (of possibly many) distinct local minimum solutions that differ primarily in the insertion point on the stable manifold of the halo orbit. This occurs because the extension of the manifold has multiple periapsis points with respect to the Earth/moon primary. The solutions are differentiated by the duration of the ballistic arc on the manifold.

The second set of transfer examples are associated with a transfer to a vertical figure-eight orbit at the interior libration L_1 of sun–Earth/moon system. These are shown in Figs. 10 and 11 along with the control and mass variations (Figs. 12 and 13) and Tables 6 and 7 show the parameters specific to these two transfers. Again, two, of possibly many, solutions are given in these figures.

A check on the solution verifies that the converged values for λ_m and λ_v at t_0 satisfy Eq. (42).

Guidance for a Halo Orbit Mission

To test the guidance technique proposed, several example test cases are discussed here. These examples test the ability of the guidance algorithm to deal with an abrupt change in the operating power of the engine and sinusoidal perturbations in the acceleration during the powered phase. The CRTBP without perturbations is used to compute the nominal optimal trajectory. We assume that

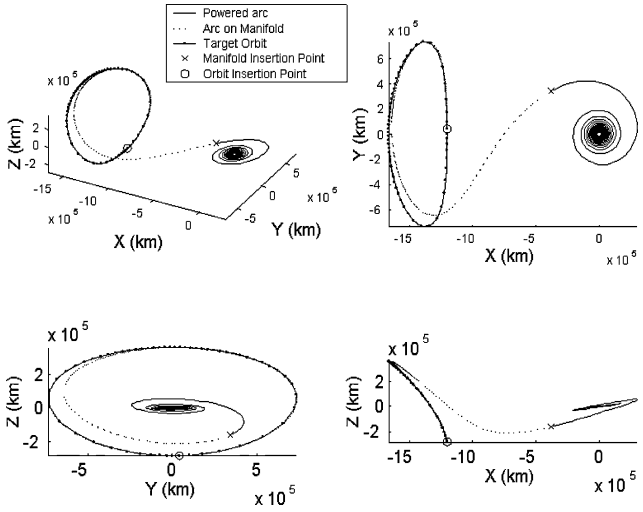

Fig. 6 Earth to halo manifold VSI transfer (A).

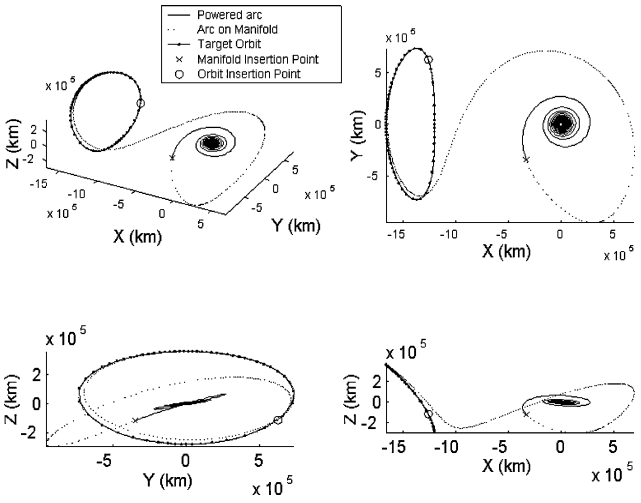

Fig. 7 Earth to halo manifold VSI transfer (B).

Table 4 Optimization and propulsion system parameters

Optimal parameter	Value	Unit	Constraint	Error	Unit
λ_m	59,780.929802428392577		e_x	0.000453004962765	km
ρ	−0.059898120893423	deg	e_y	−0.000097713433206	km
δ	−0.989205392668146	deg	e_z	0.000153216620674	km
$\dot{\rho}$	0.000018783143192	deg/s	$e_{\dot{x}}$	−0.000000000499043	km/s
$\dot{\delta}$	−0.001722190156071	deg/s	$e_{\dot{y}}$	−0.000000000104452	km/s
λ_v	5,186,657.608101757243276		$e_{\dot{z}}$	−0.000000000125772	km/s
τ	0.992 475 564 468 324	units of T	e_{mf}	0.000000001883109	kg
α	345.416498500512660	day	e_{Hf}	−0.000000000007935	
t_f	113.279693139997974	day	e_{M1}	0.006716191302985	
τ_1	21,314.496206198808068	s	e_{M2}	0.026129792444408	

Table 5 Optimization and propulsion system parameters

Optimal parameter	Value	Unit	Constraint	Error	Unit
λ_m	59,998.295923258890980		e_x	−0.000394696660805	km
ρ	−1.317067596974812	deg	e_y	−0.000519771419931	km
δ	−2.388590924138760	deg	e_z	−0.000124019992654	km
$\dot{\rho}$	0.000092983770123	deg/s	$e_{\dot{x}}$	−0.000000000096491	km/s
$\dot{\delta}$	0.001822161987009	deg/s	$e_{\dot{y}}$	0.000000001045967	km/s
λ_v	5,196,078.494123809039593		$e_{\dot{z}}$	0.000000000399279	km/s
τ	0.848 494 598 242 527	units of T	e_{mf}	0.000000000070486	kg
α	418.554138475614934	day	e_{Hf}	−0.000000000002486	
t_f	112.182827344522650	day	e_{M1}	0.018191291950643	
τ_1	42,531.922917202857207	s	e_{M2}	−0.024790387600660	

Table 6 Optimization and propulsion system parameters

Optimal parameter	Value	Unit	Constraint	Error	Unit
λ_m	67,554.835872474795906		e_x	−0.000251752091572	km
ρ	−3.541135872093880	deg	e_y	−0.000295964651741	km
δ	6.731219226553460	deg	e_z	0.000150019477587	km
$\dot{\rho}$	0.000430239724305	deg/s	$e_{\dot{x}}$	0.000000000481789	km/s
$\dot{\delta}$	0.000576557546979	deg/s	$e_{\dot{y}}$	−0.000000000288663	km/s
λ_v	5,513,589.895736707374454		$e_{\dot{z}}$	−0.000000000085545	km/s
τ	0.685 357 534 867 76	units of T	e_{mf}	0.000000005645688	kg
α	334.164950869471738	day	e_{H_f}	−0.000000000022098	
t_f	119.051551690608363	day	e_{M1}	−0.004554866347462	
τ_1	3828.262854466334375	s	e_{M2}	−0.012086209608242	

Table 7 Optimization and propulsion system parameters

Optimal parameter	Value	Unit	Constraint	Error	Unit
λ_m	61,417.474640955966606		e_x	0.005341971875168	km
ρ	−3.533323283398871	deg	e_y	0.009986697696149	km
δ	0.463336135551819	deg	e_z	−0.001380653411616	km
$\dot{\rho}$	−0.000116121239570	deg/s	$e_{\dot{x}}$	0.000000003680140	km/s
$\dot{\delta}$	−0.000629328103878	deg/s	$e_{\dot{y}}$	0.000000009855700	km/s
λ_v	5,257,172.367979603819549		$e_{\dot{z}}$	−0.000000000279905	km/s
τ	0.050170572950689	units of T	e_{mf}	0.000000110303063	kg
α	438.245341877321835	day	e_{H_f}	−0.000000000042576	
t_f	129.121171026147692	day	e_{M1}	−0.041491640033200	
τ_1	11,476.176569629435107	s	e_{M2}	0.042971774004400	

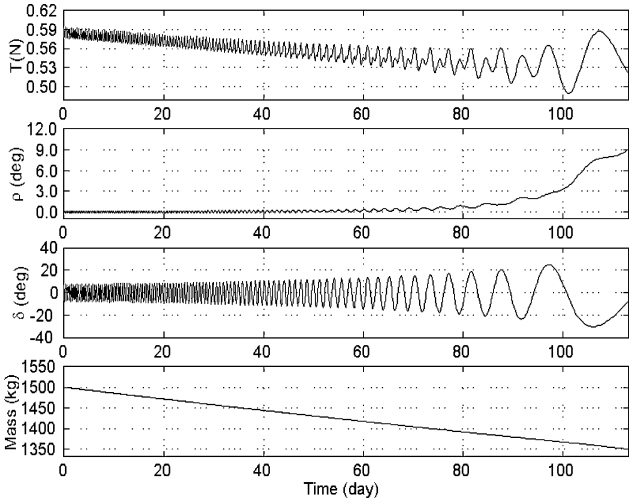

Fig. 8 Earth to halo manifold VSI transfer A: control and mass history.

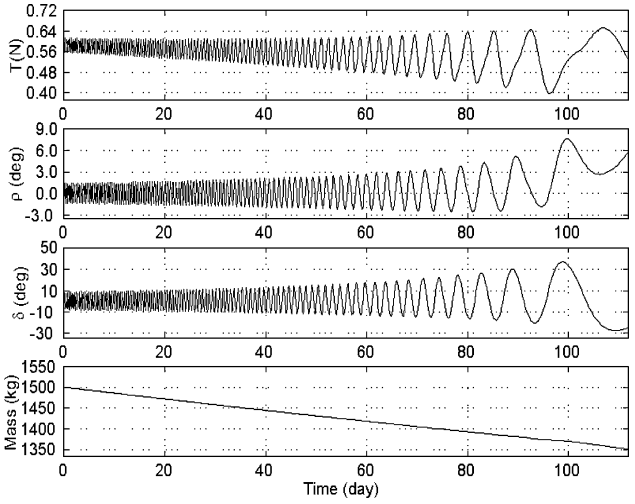

Fig. 9 Earth to halo manifold VSI transfer B: control and mass history.

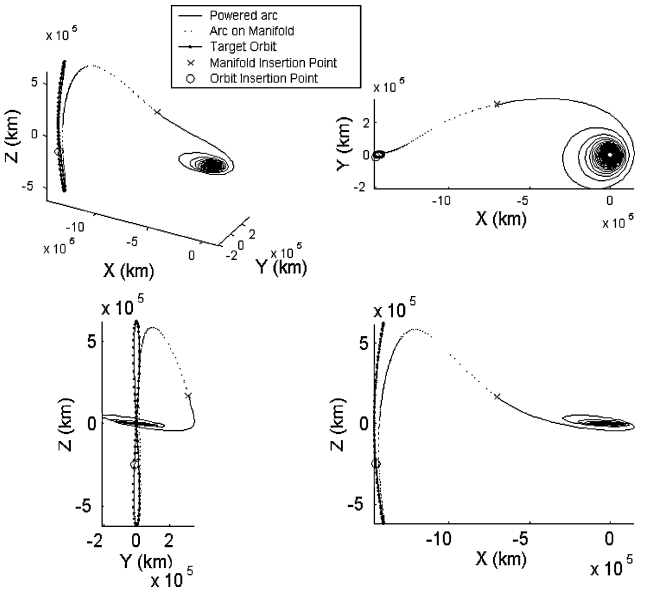

Fig. 10 Earth to vertical figure-eight manifold VSI transfer (A).

any changes to the target orbit and its manifolds are such that they remain close to the nominal orbit and its manifold.

Change in the Operating Power of the Engine

Unanticipated fluctuations in the operating power of the engine can occur during the mission. In this example a sudden change in the power of engine occurs in an arbitrary point of the powered arc. For the example presented here, the time is chosen from $t - t_0 = 20$ to 80 days, where maximum power of the engine drops from the nominal $P_{\max} = 10$ kw to $P_{\max} = 5$ kw.

The errors in position and velocity are negligible, and the variations in the thrust direction vector referenced to the vuw frame (ρ, δ) from the nominal (optimal) trajectory remain small. The main effect is in the thrust magnitude, and as a consequence the mass consumption increases. The guidance technique used can successfully guide the vehicle even with a 50% reduction in the power (see Fig. 14). Deviations in the orientation angles ρ and δ and in the spacecraft

Table 8 Parameters of the nonmodeled accelerations[24]

Perturbation	Amplitude x axis, km/s^2	Amplitude y axis, km/s^2	Amplitude z axis, km/s^2	Period, day
Mars	$0.1529e-10$	$0.0623e-10$	$0.0049e-10$	779.94
Venus	$2.0789e-10$	$0.5972e-10$	$0.1231e-10$	583.92
Jupiter	$3.6769e-10$	$2.6124e-10$	$0.0838e-10$	398.88

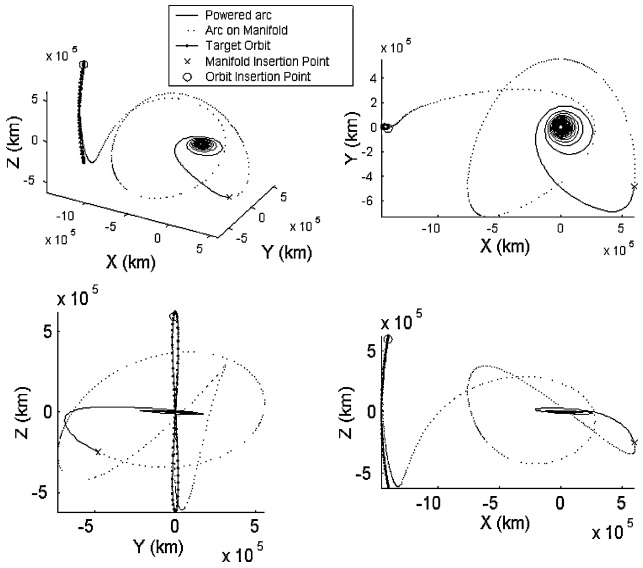

Fig. 11 Earth to vertical figure-eight manifold VSI transfer (B).

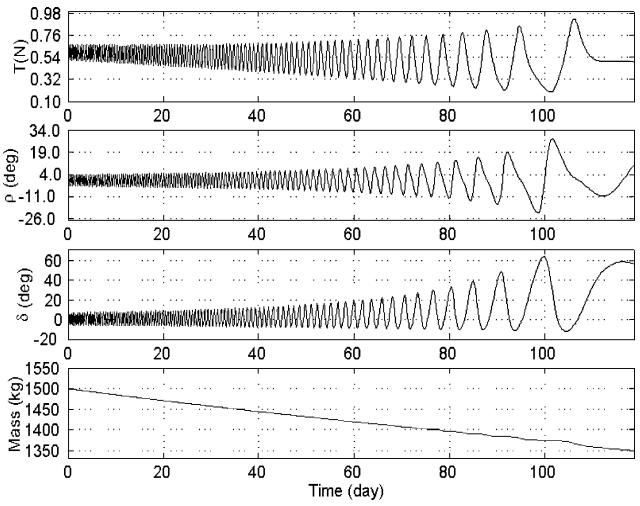

Fig. 12 Earth to vertical figure-eight manifold VSI transfer (A).

position are less than 10^{-8} (deg and km, respectively) and are not shown. Alternatively, a new trajectory for the 5000-W engine which is more effective, can be obtained, but it has to be done in real time. The idea is to track the nominal trajectory even in the case where an unanticipated power reduction occurs.

Unmodeled Accelerations

Perturbations in the acceleration will affect the spacecraft during the transfer, sinusoidal accelerations have been applied along the three axes (see Table 8) (Ref. 24).

Once the feedback controller has been designed, the frequency response of the control system will show how the frequencies of the perturbation will affect the performance of the guidance system. If some information, such as the range of frequencies of the perturbations, is known in advance, the feedback controller can be designed to filter out the effect of this set of perturbations. The gain matrix

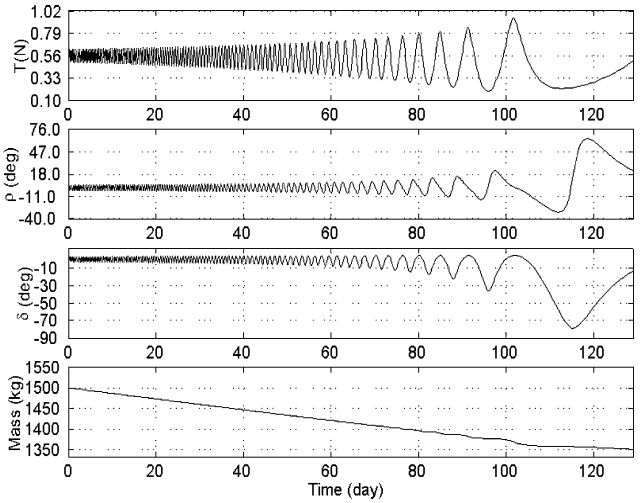

Fig. 13 Earth to vertical figure-eight manifold transfer (B).

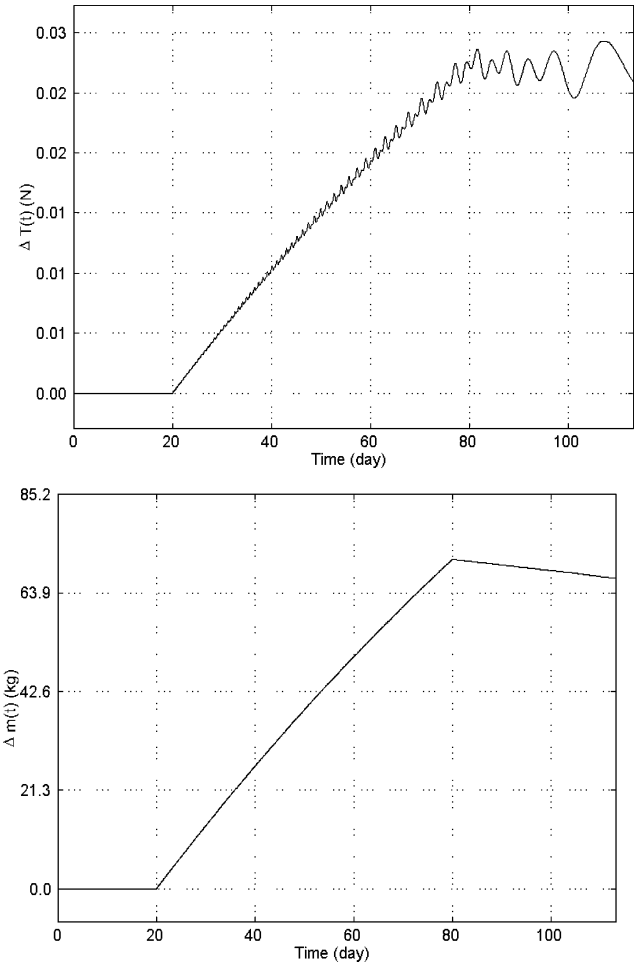

Fig. 14 Thrust and mass deviations from the nominal powered arc trajectory as a result of changes in the engine power at $t = 20$ and 80 days.

for the controller K_{TP} for the transfer phase (calculated using pole placement techniques) is given by

$$K_{TP} = \begin{bmatrix} 1.8e{-}7 & -6.9899e{-}37 & 0.0 & 6.0e{-}4 & -6.7931e{-}33 & 0.0 \\ -7.6816e{-}37 & 8.0e{-}8 & 0.0 & 2.6599e{-}33 & 4.0e{-}4 & 0.0 \\ 0.0 & 0.0 & 2.0e{-}8 & 0.0 & 0.0 & 2.0e{-}4 \end{bmatrix}$$

In Fig. 15 the time history of the main variables in the transfer phase is shown. In this case, the engine is continuously compensating for the perturbations. One of the advantages of using feedback linearization is that those results can be generalized using a frequency analysis (i.e., multivariable Bode plot). As an example, if the period of the perturbations are between $T = 10^{-5}$ and 10^5 days and the total magnitude of the perturbations in each axis are less than 1.8×10^{-9}, 8×10^{-10}, and 2×10^{-10} km/s^2, respectively, then the position error in each axis will be less than 10 m. It is not necessary to perform Monte Carlo simulations, the frequency analysis covers the range of possible perturbations.

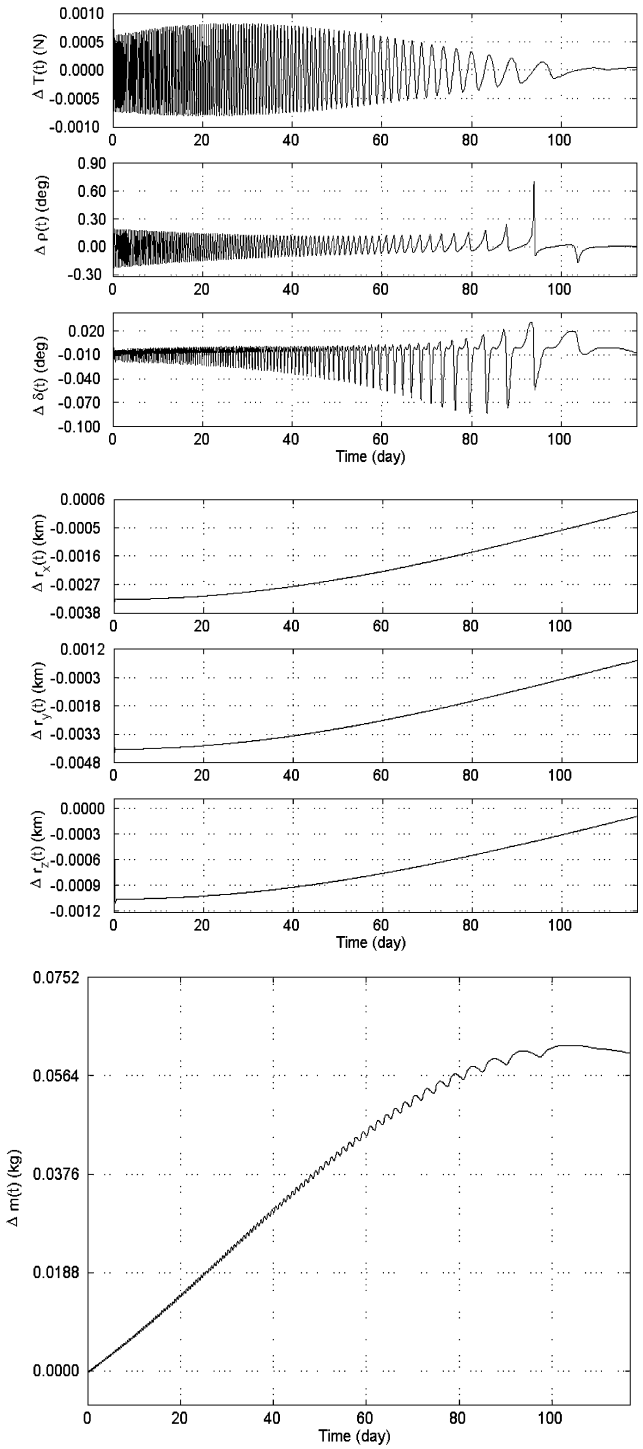

Fig. 15 Control, position, and mass deviations from the nominal powered arc trajectory as a result of periodic gravitational pertubations.

Conclusions

In this study, the first-order necessary conditions for a time-optimal, low-thrust, variable-specific-impulse transfer between a given parking orbit to the stable manifold of an unstable periodic orbit have been derived. The associated boundary problem has been solved using nonlinear root-finding and nonlinear programming algorithms, where the states and controls are continuous and the controls are based on the Pontryagin maximum principle. This methodology is applicable to any type of unstable periodic orbit in the circular restricted three-body problem force-field model. Also, a guidance algorithm that is applicable to the powered phase has been proposed, and several prototype cases have been simulated. The guidance algorithm has been shown to be capable of dealing with both power fluctuations and periodic unmodeled gravitational perturbations. These two types of perturbations have been used as an example, and the guidance algorithm is not restricted to these.

The extension of this work to quasi-periodic orbits in a realistic sun–Earth/moon model, the optimization of the parking orbit parameters, and research on optimal closed-loop returns to the nominal trajectory merit further study. Additionally, for the control on the manifold phase, the combined use of the proposed guidance scheme and the use of the stable manifold remains to be investigated. Finally, having set up a solid framework to study these types of problems, the solution of additional optimization problems are in order. These include minimum fuel transfers to the final orbit or their stable manifold and minimum time transfers to the final orbit with fixed propellant masses.

Acknowledgments

The work described here has been performed at the University of Texas at Austin and was partly supported by NASA Contract NAG9-147; the third author was partly supported by the Consejo Nacional de Ciencia y Tecnología (CONACyT). Special thanks to David Weyburn, an undergraduate Research Assistant, for his contribution in generating the necessary software and templates for some of the plots presented.

References

[1]Hull, D., *Optimal Control Theory for Applications*, Springer-Verlag, New York, 2003, pp. 221–274.

[2]Bryson, A. E., and Ho, Y., *Applied Optimal Control*, Hemisphere, New York, 1975, pp. 42–127.

[3]Marec, J. P., *Optimal Space Trajectories*, Elsevier Scientific, New York, 1979, pp. 53–70.

[4]Lawden, D. E., *Optimal Trajectories for Space Navigation*, Butterworths, London, 1963, pp. 96–124.

[5]Sastry, S., *Nonlinear Systems. Analysis, Stability and Control*, Springer-Verlag, New York, 1999, pp. 384–509.

[6]Guckenheimer, J., and Holmes, P., "Nonlinear Oscillations, Dynamical Systems, and Bifurcations of Vector Fields," *Applied Mathematical Sciences*, Vol. 42, edited by F. John, Springer-Verlag, New York, 1991, pp. 12–27.

[7]Gomez, G., Jorba, A., Masdemont, J., and Simo, C., "Study of the Transfer from the Earth to a Halo Orbit Round the Equilibrium Point L1," *Celestial Mechanics and Dynamical Astronomy*, Vol. 56, Aug. 1993, pp. 541–562.

[8]Breakwell, J., and Brown, J. V., "The Halo Family of 3-Dimensional Periodic Orbits in the Earth-Moon Restricted 3-Body Problem," *Celestial Mechanics*, Vol. 20, Nov. 1979, pp. 389–404.

[9]Howell, K. C., Barden, B., and Lo, M., "Application of Dynamical Systems Theory to Trajectory Design for a Libration Point Mission," *Journal of the Astronautical Sciences*, Vol. 45, No. 2, 1997, pp. 161–178.

[10]Serban, R., Koon, W. S., Lo, M., Marsden, J., Petzold, L. R., Ross, S. D., and Wilson, R., "Optimal Control for Halo Orbit Missions," International Federation of Automatic Control Meeting, Princeton, NJ, March 2000.

[11]Whiffen, G. J., and Sims, J. A., "Application of the SDC Optimal Control Algorithm to Low-Thrust Escape and Capture Trajectory Optimization," *Proceedings of the AAS/AIAA Space Flight Mechanics Meeting*, Vol. 112, Univelt, 2002, pp. 1361–1382.

[12]Sims, J. A., Whiffen, G. J, Finlayson, P. A., and Petropoulos, A. E., "Low-Thrust Orbit Transfer Around Minor Planets," *Proceedings of the AAS/AIAA Space Flight Mechanics Meeting*, Vol. 112, Univelt, 2002, pp. 541–552.

[13]Mitchell, J. W., and Richardson, D. L., "Invariant Manifold Tracking for First-Order Nonlinear Hill's Equations," *Journal of Guidance, Control, and Dynamics*, Vol. 26, No. 4, 2003, pp. 622–627.

[14]Renault, C. A., and Scheeres, D. J., "Optimal Placement of Statistical Maneuvers in an Unstable Orbital Environment," *Journal of Guidance, Control, and Dynamics*, Vol. 26, No. 5, 2003, pp. 758–769.

[15]Howell, K. C., and Marchand, B. G., "Control Strategies for Formation Flight in the Vicinity of the Libration Points," *Proceedings of the AAS/AIAA Space Flight Mechanics Meeting*, Vol. 114, Univelt, 2003, pp. 197–238.

[16]Szebehely, V., *Theory of Orbits: The Restricted Problem of Three Bodies*, Academic Press, New York, 1967, pp. 7–22.

[17]Henon, M., "Numerical Exploration of the Restricted Problem VI. Hill's Case: Non-Periodic Orbits," *Astronomy and Astrophysics*, Vol. 9, Nov. 1970, pp. 24–36.

[18]Villac, B. F., and Scheeres, D. J., "A Simple Algorithm to Compute Hyperbolic Invariant Manifolds Near L_1 and L_2," *Proceedings of the AAS/AIAA Space Flight Mechanics Meeting*, AAS Paper 04-243, Feb. 2004.

[19]Ocampo, C., "Finite Burn Maneuver Modelling for a Generalized Trajectory Design and Optimization System," *Astrodynamics, Space Missions, and Chaos, Annals of the New York Academy of Sciences*, Vol. 1017, 2004.

[20]Pontryagin, L. S., Boltyanskii, V. G., Gamkrelidze, R. V., and Mischchenko, E. F., *The Mathematical Theory of Optimal Processes*, Wiley-Interscience, New York, 1963, pp. 1–114.

[21]Dixon, L. C., and Bartholomew-Biggs, M. C., "Adjoint Control Transformations for Solving Practical Optimal Control Problems," *Optimal Control Applications and Methods*, Vol. 2, No. 4, 1981, pp. 365–381.

[22]"Archives of the Harwell Subroutine Library," AEA Technology, Harwell Lab., Oxfordshire, England, U.K., Dec. 1995.

[23]Pu, C. L., and Edelbaum, T. N., "Four Body Trajectory Optimization," *AIAA Journal*, Vol. 13, No. 3, 1975, pp. 333–336.

[24]Evans, S. W. (ed.), "Natural Environment Near the Sun–Earth/Moon L2 Libration Point," Next Generation Space Telescope Doc-0761, NASA Marshall Space Flight Center, AL, Sept. 2000.